The dual inhibition of RNA Pol I transcription and PIM kinase as a new therapeutic approach to treat advanced prostate cancer

Authors: Richard J Rebello[1], Eric Kusnadi[2], Don Cameron[2], Helen Pearson[2], Analia Lesmana[2], Jennifer Devlin[2], Denis Drygin[3], Ashlee K Clark[1], Laura Porter[1], John Pedersen[4], Shahneen Sandhu[5], Gail P Risbridger[1], Richard B Pearson[2,4,6,7,*], Ross D Hannan[2,4,5,6,8,9,*], Luc Furic[1,*]

Affiliations:

[1] Cancer Program, Biomedicine Discovery Institute and Department of Anatomy & Developmental Biology, Monash University, VIC, Australia

[2] Oncogenic Signaling and Growth Control Program, Peter MacCallum Cancer Centre, St Andrews Place, East Melbourne, VIC, 3006, Australia.

[3] Pimera, Inc. San Diego, CA 92121, USA

[4] TissuPath Pathology, Melbourne, VIC, 3149, Australia

[5] Sir Peter MacCallum Department of Oncology, University of Melbourne, Parkville, VIC, 3010, Australia.

[6] Department of Biochemistry and Molecular Biology, University of Melbourne, Parkville, VIC, 3010, Australia.

[7] Department of Biochemistry and Molecular Biology, Monash University, VIC, 3800, Australia

[8] Department of Cancer Biology and Therapeutics, The John Curtin School of Medical Research, The Australian National University, ACT, 2601 Australia

[9] School of Biomedical Sciences, University of Queensland, Brisbane, Queensland 4072, Australia.

Running title: Therapeutic efficacy of inhibiting Pol I and PIM in PC

Keywords: MYC signalling; patient-derived xenografts; ribosome biogenesis; cellular responses to anticancer drugs

Financial support: This work was supported by Cancer Australia (CA 1084546 to R.D.H, R.B.P. G.P.R and L.F.); Prostate Cancer Foundation of Australia (YI 0310 to L.F. and CG 1511 to R.B.P, R.D.H and L.F. and YIA to S.S.); National Health and Medical Research Council (Program Grant 1053792 and Project Grant 1004881 to R.B.P. and R.D.H.; Senior Research Fellowships to R.B.P. and R.D.H and Senior Principal Research Fellowship APP 1102752 to G.P.R).

Conflicts of interest: The authors declare that they have no competing interests.

[*]**Correspondence to:** Luc Furic (luc.furic@monash.edu), Ross D Hannan (ross.hannan@anu.edu.au), Richard B Pearson (rick.pearson@petermac.org)

Translational Relevance

Metastatic castrate-resistant prostate cancer (mCRPC) is the most aggressive stage of the disease and remains incurable, highlighting the need for new therapeutic targets. Prostate epithelium is exquisitely sensitive to MYC activity and accordingly MYC is almost universally overexpressed in mCRPC. Unfortunately, the development of therapeutic agents directly targeting MYC has been largely unsuccessful, thus emphasizing the indirect targeting of MYC activity through inhibition of downstream cellular processes. One of these key processes in cancer cells is to accelerate proliferative growth via stimulation of high levels of ribosome biogenesis through regulation of RNA polymerase I (Pol I). MYC also regulates and cooperates with PIM kinases to increase the activity of the eIF4F translation initiation complex. Here, we provide preclinical evidence that co-targeting Pol I transcriptional activity and PIM kinases is an effective means of inhibiting MYC-driven prostate cancer. We employ numerous models of PC including a novel CRPC patient derived xenograft system which shows the pre-clinical efficacy of therapies that combine to target MYC directed signaling to the ribosome.

Abstract:

Purpose: The MYC oncogene is frequently over-expressed in prostate cancer (PC). Upregulation of ribosome biogenesis and function is characteristic of MYC-driven tumors. Additionally, PIM kinases activate MYC signaling and mRNA translation in PC and cooperate with MYC to accelerate tumorigenesis. Here, we investigate the efficacy of a single and dual approach targeting ribosome biogenesis and function to treat PC.

Experimental design: The inhibition of ribosomal RNA (rRNA) synthesis with CX-5461, a potent, selective and orally bioavailable inhibitor of RNA polymerase I (Pol I) transcription has been successfully exploited therapeutically, but only in models of hematological malignancy. CX-5461 and CX-6258, a pan-PIM kinase inhibitor, were tested alone and in combination in PC cell lines, in Hi-MYC and PTEN-deficient mouse models and in patient derived xenografts (PDX) of metastatic tissue obtained from a castration-resistant PC patient.

Results: CX-5461 inhibited anchorage-independent growth and induced cell cycle arrest in PC cell lines at nanomolar concentrations. Oral administration of 50 mg/kg CX-5461 induced p53 expression and activity and reduced proliferation (Ki-67) and invasion (loss of ductal actin) in Hi-MYC tumors, but not in PTEN null (low MYC) tumors. While 100 mg/kg CX-6258 showed limited effect alone, its combination with CX-5461 further suppressed proliferation and dramatically reduced large invasive lesions in both models. This rational combination strategy significantly inhibited proliferation and induced cell death in PDX of PC.

Conclusion: Our results demonstrate preclinical efficacy of targeting the ribosome at multiple levels and provide a new approach for the treatment of PC.

Introduction

One-in-seven men will be diagnosed with prostate cancer (PC) in their lifetime and PC related deaths is above twenty thousand per year in the US (1). PC is driven by androgen receptor (AR) activation, making androgen deprivation therapy (ADT) the mainstay of treatment for men with advanced PC. Despite initial efficacy, patients inevitably relapse despite castrate levels of serum testosterone, a lethal condition known as castrate-resistant prostate cancer (CRPC) (1, 2). Targeted therapies to manage PC are limited to AR signaling, although recent clinical trials are assessing the therapeutic efficacy of inhibiting the PI3K/mTORC1 pathway(2). Overexpression of the MYC oncogene is among the most common alterations in PC, with over 30 percent of localized and a majority of CRPC tumors showing MYC overexpression (3, 4). MYC controls cell growth by transcriptionally upregulating components involved in ribosome biogenesis, including direct binding to ribosomal RNA (rRNA) genes, which hyper-activates the synthesis of rRNA (5-7).

In PC, MYC expression positively correlates with the overexpression of rRNA (8). Additionally, the PIM kinases, consisting of three paralogs (PIM1, 2, 3) with pro-oncogenic activities, were shown to be concurrently over-expressed with MYC in PC (9). PIM kinases increase MYC transcriptional activity (10) and stability (11), they also stimulate eIF4E-dependent mRNA translation through stimulation of 4E-BP1 phosphorylation at serine 65 (12). This accelerates prostate tumor growth and mediates resistance to conventional therapies (13-15). It has been documented that MYC-driven hematological cancers are sensitive to inhibition of eIF4E-dependent mRNA translation (16). Therefore, we hypothesized that targeting ribosome biogenesis and function by inhibiting Pol I transcriptional activity alone, or in combination with

inhibitors or modulators of mRNA translation (such as PIM kinases) may represent a novel method of treating MYC-driven PC.

Here, we demonstrate the efficacy of a novel small molecule inhibitor of Pol I transcription, CX-5461, in inhibiting growth, colony formation and in inducing cell death in human PC cells. Using a genetically engineered mouse model (GEMM) of PC, the Hi-MYC model (17), we demonstrate that CX-5461 suppresses tumor progression *in vivo*. Strikingly, CX-5461 in combination therapy with the pan-PIM kinase inhibitor CX-6258, lead to a reversion of Hi-MYC tumors back to high grade intraepithelial neoplasia (HGPIN). This correlated with repression of ribosome biogenesis (reduced rRNA synthesis) and ribosome function (reduced 4EBP1 phosphorylation). Furthermore, and as a proof of principle of promising preclinical efficacy, this combination therapy prevented tumor growth in a GEMM of PTEN depletion and a PDX model of aggressive high-MYC PC unresponsive to conventional therapy.

Materials and Methods

Cell culture

Authenticated PC-3, DU145 and LNCaP human prostate cell lines were purchased from the American Type Culture Collection and cultivated in RPMI supplemented with 10% FBS. BM67 mouse prostate epithelial cells were generated from PBiCre$^{+/-}$;Pten$^{fl/fl}$ mice and validated as outlined previously (18). The HM-5 mouse prostate cell line was generated from a 5 month old male FVB-Tg(ARR2/Pbsn-MYC) lateral prostate. Briefly, lateral prostate lobes were isolated and minced into 5 mm3 pieces and digested at 37ºC for 2 hours in DMEM medium containing HEPES and 1 mg/ml collagenase (Sigma-Aldrich, USA). Post-digestion, prostate pieces were washed in Phosphate-buffered saline (PBS), then transferred to a 100 mm plasma gas treated tissue culture dish (BD Biosciences, USA). Cells were grown in growth medium containing

RPMI supplemented with 10% FBS (Invitrogen, USA), human recombinant epithelial growth factor (life technologies, USA), Bovine Pituitary Extract (life technologies, USA), Insulin (Sigma-Aldrich, USA), Penicillin/Streptomycin (P/S) and 10 nM testosterone (T) (Sigma-Aldrich, USA) and Y-27632 (Sigma-Aldrich, USA) and the media was replaced every 4 days. Colonies were isolated then maintained in RPMI containing 5% FBS, P/S and 10 nM T and kept in a humidified incubator at 37ºC with 5% CO2.

Inhibitors

CX-5461 and CX-6258 were generous gifts from Cylene Pharmaceuticals (San Diego, CA). RAD001 was purchased from Selleck Chemicals (Houston, TX).

Anchorage-independent growth assays

PC3 and DU145 cells were seeded into 6-well plates as single cell suspensions in 0.35% sterile low melt agarose (Bioline, USA) on a 0.7% agarose base layer and incubated overnight as described previously (19). These plates were then cultured for 3 weeks to allow colony suspensions to form.

Cell cycle analysis

Seeded PC-3 and DU145 cells were serum starved for 24 hours prior to incubation with inhibitors in order to synchronise the cell cycle at G0 phase of the cell cycle. Cells were fixed in 70% ethanol, stained with Propidium Iodide (PI) and analysed 24 hours after incubation with inhibitors on an LSR Fortessa Cell Analyser (BD Biosciences, USA).

Animal experiments

Hi-MYC (ARR2pbsn-MYC) mice were obtained from NCI-Frederick, USA and PTEN-deficient (PBiCre+/-;PTENfl/fl) mice were obtained from a breeding colony established at the Peter

MacCallum Cancer Centre, Australia. Transgenic Hi-MYC female mice were crossed with wild-type male mice to generate transgenic Hi-MYC male progeny. PBi-Cre transgenic mice (20) were crossed with PTEN floxed animals (21) to specifically deplete PTEN within the prostate epithelium. Animals were maintained on a pure FVB/N background. Both Hi-MYC and PTEN mice were aged to 4 months and given oral doses of inhibitor, bi-weekly over 4 weeks (9 doses). For acute experiments, a single dose of inhibitor was administered over 24 hours. All Hi-MYC and PTEN-deficient animals were humanely killed at 5 months of age, 24 hours after the final dose of inhibitor.

Histology & immunohistochemistry (IHC)

Lateral prostate lobes were isolated from animals 24 hours post therapy and fixed in formalin for 48 hours before histological processing. Entire prostate lobes were sectioned at 5 μm thick and every 20th section was stained with hematoxylin & eosin (H&E) (Dako, Denmark) to visualise pathological progression of disease and tumor foci. These sections were scored for percentage of invasive lesions by at least two experimenters blind to the genotype and treatment groups. Following antigen retrieval, sections were incubated with primary antibody. Primary antibody dilutions are as follows; MYC (1:600 (1 hr), Abcam (Y69)), Ki67 (1:400 (1 hr), Leica Biosystems), α-Smooth Muscle Actin (α-SMA) (1:10,000, Sigma), Phospho-ribosomal protein S6 (p-rpS6) (1:3000, Cell Signaling). Following washing, sections were incubated in Dako Envision goat α-mouse or goat α-rabbit immunoglobulins as appropriate for 1 hour at room temperature (Dako, Denmark). Staining was then visualised with choromogen DAB (Di-amino benzidene) (Dako, Denmark) for up to 5 minutes before counterstaining with hematoxylin. Stained slides were digitised using an Aperio AT Turbo slide scanner (Leica biosystems, USA).

Positively stained cells were quantified with counting algorithms provided by Aperio Image Scope analysis software (Leica Biosystems, USA)

Western blotting

Protein extracts were isolated by lysis in passive lysis buffer solution (Progen, USA). Whole animal prostate lobe tissues were ground into a powder in liquid nitrogen using a pre-chilled mortar and pestle and protein lysates were prepared by dissolving the powdered tissue in SDS lysis buffer. A detailed description is provided in supplemental methods.

Ribosomal RNA extraction and q-PCR

Isolated prostate lobes were snap frozen and maintained at -80ºC until analysed. Tissue was homogenised by crushing in liquid nitrogen, then cells were lysed and the RNA extracted using then NucleoSpin kit (Macherey-Nagel, Germany). SuperScript III Reverse Transcriptase (Thermo Fisher, USA) was used to synthesise cDNA from 1 ug of RNA/sample. The qPCR reactions were performed with Fast SYBR-Green Master Mix (Applied Biosystems, USA) on the StepOnePlus Real-Time PCR Instrument (Applied Biosystems, USA). Expression of both the 45S pre-rRNA and p21 were normalised to housekeeping gene B2M. All primer sets have been previously published **(22, 23)** and are as follows: pre-rRNA for: CCA AGT GTT CAT GCC ACG TG; pre-rRNA rev: CGA GCG ACT GCC ACA AAA A; p21 for: AAT ACC GTG GGT GTC AAA GC; p21 rev: GTG TGA GGA CTC GGG ACA AT; B2M for: TTC ACC CCC ACT GAG ACT GA; B2M rev: GTC TTG GGC TCG GCC ATA.

Statistical analysis

Graphpad Prism software was used to generate graphs and perform statistical analyses and significance of data. *In vitro* experiments were performed in triplicate and expressed as a

summary of the mean of replicates with standard deviation (SD), unless specified otherwise. Histological quantitation of mouse prostate tissue was performed using an Aperio ScanScope digital scanner and viewed using ImageScope software (Aperio).

Animal Ethics

All animal experiments were performed according to protocols approved by the Monash University Animal Ethics Committee, Monash University.

Patient derived xenografts

Human tissues were obtained post-mortem during autopsy. Tissue collection was performed according to approved Human ethics (Peter MacCallum Cancer Centre). Tumor grafts were implanted under the renal capsule of immunodeficient mice (NSG) according to our previously published protocol (24) with the following modifications: tissue was sectioned in thin 0.3 mm slices using a Krumdieck tissue slicer MD6000 (TSE systems, Germany) and grafted under the renal capsule without adding seminal vesicle mesenchymal cells or prostate fibroblasts. Grafts were allowed to establish in testosterone supplemented hosts for a period of 3 weeks prior to treatment. Host mice were treated with vehicle or CX-5461/CX-6258 combination and given 4 doses over 9 days. Mice were humanely killed 24 hours after the last dose and grafts were harvested. Grafted tissues were measured, weighed and fixed in 10% formalin for 24 hours prior to being processed and embedded in paraffin.

Results

PC cells are sensitive to CX-5461, an inhibitor of RNA Pol I transcriptional activity

MYC loci amplification is observed in more than 30 percent of PC and MYC protein is almost universally overexpressed in metastatic CRPC (4). Accordingly, high levels of MYC protein expression are observed in primary human prostate epithelial (HPE) cells isolated from patient tissue (HPE-1, HPE-2) and in immortalized PC cells; LNCaP, PC3 and DU145 (Figure 1A). Conversely, MYC expression is relatively low in BM67 cells, a murine prostate epithelial cancer cell line isolated from the PB-Cre;$PTEN^{Flox}$ mouse model of PC (Figure 1A, S1A) (18). HM-5 cells isolated from the Hi-MYC PC mouse model (18) express high levels of MYC (Figure 1A, S1A). To determine if inhibition of Pol I transcription has therapeutic potential in PC, we tested the ability of CX-5461 to suppress anchorage-independent growth of PC cells in culture. PC3 and DU145 cells, which are derived from aggressive metastatic PC, form colonies when seeded in soft agar. Cells were treated with increasing concentrations of CX-5461. While a 50 nM concentration did not significantly impair colony formation, 200 nM suppressed the number of colonies significantly in both cell lines: by 83% in PC3 (Figure 1B) and 92% in DU145 ($n=3$, $P<0.001$) (Figure 1C), demonstrating in vitro efficacy of CX-5461 in suppressing anchorage-independent growth of PC cells.

To determine if the impairment of colony formation was due to cytotoxic or cytostatic effects of CX-5461, we performed cell cycle analysis of PC3, DU145 and LNCaP cells treated with increasing concentrations of CX-5461 (Figure 1D-F). Treatment of PC3 (Figure 1D) and DU145 cells (Figure 1E) with concentrations of CX-5461 ranging from 50 nM to 1000 nM CX-5461 did not significantly increase cell death, as measured through sub-G1 content. In PC3 and DU145 cells, a concentration of 200 nM and 500 nM of CX-5461, respectively, induced a cell cycle

arrest characterized by accumulation of cells in G2-M (Figure 1D-E). However, LNCaP cells were 7 to 15 times more sensitive to CX-5461 than PC3 and DU145 cells, respectively (Figure 1F), with a 30nM concentration sufficient to induce cell cycle arrest and accumulation in G2/M phase, again without induction of cell death. One determinant of sensitivity to CX-5461 is p53 activity (22). Both PC3 and DU145 cells are p53 null while LNCaP cells express functional p53 (25). Accordingly, phosphorylated p53 accumulation was observed in LNCaP cells at 2 hours following treatment with CX-5461 (Figure 1G). This p53 accumulation was also accompanied by an increase in p21 at 8 and 24 hours post-treatment (Figure 1G). These results show that CX-5461 is cytostatic in PC cell lines, arresting cells in G2M. The lack of apoptosis is not simply due to the lack of p53 as LNCaP also arrest in G2M despite activating a p53 response. These data are consistent with our earlier studies demonstrating that in solid tumors therapeutic efficacy of CX-5461 does not correlate with p53 status (26), but can promote sensitivity when present. Together, these results demonstrate that PC cells are sensitive to Pol I transcription inhibition in vitro, leading to significant cell cycle arrest that abrogates colony formation.

RNA polymerase I activity inhibition suppresses tumor progression in MYC-driven prostate cancer, in vivo

In order to evaluate CX-5461 potential to prevent disease progression in vivo, we employed a GEMM that faithfully recapitulates human disease progression from PIN to invasive carcinoma. GEMM of PC have the advantage of developing autochthonous tumors at high penetrance and with reproducible kinetics. To test if the sensitivity of PC cell lines to Pol I transcription inhibition would translate to a therapeutic effect in vivo we tested CX-5461 in the Hi-MYC mouse (17). The Hi-MYC mouse reproduces the pathological development of human PC. In this model, MYC expression is under the control of the probasin promoter, which is prostate-specific

and androgen-dependent. Neoplastic lesions develop initially in the ventral and lateral lobes (17). High grade intra-epithelial neoplasia (PIN) is observed at 2 months of age; in situ carcinoma is fully penetrant at 5 months of age. We followed disease progression at various time points (Figure 2A) and our observations show a reproducible and highly penetrant phenotype. At 5 months of age we observed the development of multiple invasive lesions while, by 8 months, invasive lesions occupied most of the ventral and lateral lobes (Figure 2A). This is characterized by the loss or fragmentation of the smooth muscle actin layer surrounding the prostatic ducts, as previously reported (17, 27). Hi-MYC tumors are highly proliferative (17) and quantitation shows that 50% of luminal epithelial cells over-express MYC (Figure 2B) with a high proliferative index marked by Ki-67. This is evident by 2 months of age, maintained at 5 months and then reduced by 8 months as tumors become highly compacted with ductal lumen entirely filled with tumor cells (Figure 2B). Considering that proliferation peaks and invasive lesions develop at 5 month of age, we selected this time point as the most suitable for determining efficacy of Pol I inhibition on proliferation and invasion in this model.

Five month old Hi-MYC mice (n=3 per group) were treated with CX-5461 at a dose of 50 mg/kg. This dose was previously shown to induce therapeutic effects in a MYC-driven murine model of lymphoma (22). Following 24 hours of treatment lateral prostate tissue was isolated and analyzed for Pol I transcription rate by measuring the abundance of the 45S pre-ribosomal RNA (rRNA) (Figure 2C) and for induction of p53 (Figure 2D), which is a known marker of the immediate response to RNA Pol I transcription inhibition in p53 WT tumors in vivo (22). Animals treated with CX-5461 for 24 hours displayed a significant reduction (66% ± 26%) in the amount of 45S pre-rRNA (Figure 2C) (n=3, P=0.048), which correlated with a robust accumulation of p53 in the same tissues (Figure 2D). We then examined the therapeutic effect of

a longer term dosage of CX-5461 in Hi-MYC mice. Four-month old Hi-MYC mice were dosed twice weekly for 4 weeks, with 50 mg/kg CX-5461 for a total of 9 doses (n=3 per group). At sacrifice, lateral prostate tissue was harvested and analyzed by IHC. While the number of MYC expressing epithelial cells were not significantly reduced in these tissue sections (Figure 2E, F), Ki-67 expression was reduced by 50% (n=3 per group, P=0.024), indicating that the proliferative capacity was significantly repressed (Figure 2G, H). This striking reduction in the proliferative potential of Hi-MYC tumors confirms the *in vivo* efficacy of CX-5461 in solid tumors and supports the *in vitro* results obtained with PC cell lines showing cell cycle arrest.

Co-targeting PIM kinase activity potentiates the effect of RNA polymerase I activity inhibition in prostate cancer cells.

As previously mentioned, PIM-1 is co-elevated with MYC in human and Hi-MYC prostate adenocarcinoma, where it is believed to accelerate tumorigenesis (17). It was recently shown that resistance to therapy with the mTORC1 inhibitor, RAD001, is mediated by up-regulated signaling via eukaryotic initiation factor 4E binding protein-1 (4E-BP1) in Hi-MYC mice (15, 28), a PIM kinase substrate (29). Additionally, a PIM inhibitor has been reported recently to have efficacy in a model of MYC-driven prostate cancer (30). We therefore examined whether suppressing ribosome biogenesis with CX-5461 and PIM kinase activity co-operate in PC inhibition. Firstly, we tested the efficacy of CX-6258, a novel pan-PIM inhibitor (31) in inhibiting anchorage-independent growth of PC3 and DU145 cells. CX-6258 significantly suppressed colony formation of PC3 and DU145 cells (n=3, $P<0.001$) (Figure 3A, B). Cell cycle analyses of LNCaP cells 48 hours following CX-6258 treatment revealed a significant decrease in G0/G1 phase and a pronounced accumulation of cells in G2/M phase (Figure 3C). Consistent with previous studies showing that PIM kinases regulate 4E-BP1, western blotting analysis

demonstrated that phosphorylation on serine 65 (S65) of 4E-BP1 was reduced (Figure 3D), along with a dramatic shift of hyper-phosphorylated 4E-BP1 (top arrow) to hypo-phosphorylated (bottom arrow) total 4E-BP1 within 2 hours of treatment with 5 and 10 μM CX-6258 only and not with CX-5461 (Figure 3D). Combined treatment of PC3 and DU145 cells with 50 nM of CX-5461 and CX-6258 significantly reduced anchorage-independent growth compared to single agents (Figure 3E, F). Cell cycle analysis revealed that LNCaP and DU145 cells treated with a combination of agents exhibited a significant arrest in G2/M phase than what was observed with either agent alone (Figure 3G, H).

To further examine the potential cooperative effects of combined Pol I transcription inhibition and PIM kinase inhibition in the context of MYC driven PC, we generated an epithelial cell line from a 5-month old Hi-MYC mouse lateral prostate adenocarcinoma (HM-5) (Figure S1). HM-5 cells treated with CX-5461 for 4 hours showed a dose-dependent decrease in 45S pre-rRNA abundance ($n=3$, $P<0.05$) (Figure 4A), which correlated with a robust induction of p53 (Figure 4B) and the p53 target gene, p21, which mediates cell cycle arrest (Figure 4C). HM-5 cells treated with 100 nM CX-5461 for 24 hours showed significant accumulation in G2/M phase (Figure 4D). Conversely, HM-5 cells treated with 500 nM of CX-6258 showed a marked increase of cells in G0/G1 phase of the cell cycle ($n=3$, $P< 0.01$) (Figure 4D), consistent with the effects seen with other growth factor signaling pathway inhibitors (32). While the combination of inhibitors show significant G2/M accumulation of cells consistent with CX-5461 single agent effect. This strongly suggests that, even though PIM suppression via CX-6258 does not initiate G2/M arrest alone in these cells, it does not prevent CX-5461 induced G2/M suppression indicating that G2/M arrest is dominant. Western blot analysis of HM-5 cells treated with 500 nM CX-6258 showed a marked reduction in 4E-BP1 phosphorylation at s65 and almost complete

suppression at a concentration of 5000 nM CX-6258 (Figure 4E). The combination effect was assessed in HM-5 cells by allowing them to proliferate in the presence of low, sub-lethal doses of each inhibitor. A concentration of 10 nM CX-5461 was found to co-operate with 200 nM CX-6258 to reduce the number of cells after 72 hours incubation, significantly more than cells grown in the presence of vehicle or either inhibitor alone (Figure 4F). Additionally, this combination resulted in a significant reduction in the number of colonies formed as compared with vehicle or single agent treated cells (Figure 4G). Viability of HM-5 cells was assessed after 72 hours incubation with CX-5461, CX-6258 or in combination and showed that indeed these drugs co-operate to induce cell death at this concentration (Figure 4H). Together, this data demonstrates that combined Pol I transcription inhibition and PIM kinase inhibition co-operates in vitro to enhance efficacy of each inhibitor in Hi-MYC tumor cells.

Co-targeting RNA Pol I and PIM in the Hi-MYC and the PTEN-deficient models of PC

We next examined whether the robust effect of combining Pol I inhibition with PIM inhibition on MYC-driven PC in vitro translated to an improved therapeutic outcome in vivo. To test this, four-month old Hi-MYC mice were treated with single agents or combination therapy for 4 weeks, bi-weekly, and the effect of therapy on lateral prostate adenocarcinoma were analyzed via histopathological assessment and IHC with 8-11 animals per treatment group (Vehicle: n=11, CX-5461: n=8, CX-6258: n=8, combination: n=11).

Animals on combination therapy had a markedly improved phenotype, displaying HGPIN as the most prevalent lesion compared with vehicle alone or either inhibitor alone (Figure 5A). While assessing the occurrence of invasive lesions in the same groups, we observed that CX-5461 alone drastically reduced the number of invasive lesions (Figure 5B). There was no striking difference in the histopathology of lesions in CX-6258 treated animals compared with animals treated with

vehicle only, indicating that inhibiting PIM alone may have limited impact in preventing MYC induced adenocarcinoma. Similar to CX-5461 alone, combination therapy suppressed the incidence of invasive foci in almost all treated animals (9/11 animals) (Figure 5B). In addition, cell proliferation, as marked by Ki-67, was significantly lower in animals treated with combination therapy as compared with other groups (Figure 5C). These results highlight the fact that PIM co-operates with MYC but does not direct MYC oncogenic influence completely. Importantly, there was no impact on body weight of animals in any of the treatment groups, indicating these drugs were well tolerated in combination (Figure S2) and provide a novel and potent therapeutic approach to treat PC. In contrast with these findings, but in agreement with results reported by Clegg and colleagues (28), no cooperativity was observed *in vivo* in Hi-MYC mice when combining CX-5461 with RAD001, a partial inhibitor of mTORC1 (Figure S3).

We then examined whether this robust combination effect could be validated in another GEMM of PC by employing the conditional PTEN-KO model (33, 34), where MYC expression is comparatively low. Again, four-month old PTEN-deficient mice were treated for 4 weeks, bi-weekly, and the effect of therapy on anterior prostate carcinoma were analyzed via histopathological assessment with 4 animals per treatment group for the total percentage of carcinoma. Unlike the Hi-MYC model, we did not observe invasive adenocarcinoma in any tissue sections and the highest grade lesion observed was carcinoma *in situ* (CIS) (Figure 5D) which is consistent with previous characterization of this GEMM (33). In contrast with the Hi-MYC model, we observed no significant histological differences in animals treated with CX-5461 alone. This difference in response between these two models most likely stems from a lower dependence on MYC as a driver of tumorigenesis in the PTEN-deficient mouse and thus low levels of MYC do not sensitize these tumors to Pol I inhibition as a single agent. However,

we observed a decreased incidence of carcinoma *in situ* (CIS) in animals treated with CX-6258 alone and a striking decrease in tumor burden after combination treatment (Figure 5D). Animals receiving the combination therapy had a ~50% decrease in incidence of CIS (P=0.03) (Figure 5E) and displayed HGPIN as their predominant pathology (Figure 5D). These observations are consistent with recent evidence that PIM kinases regulate PI3K signaling through indirect mTORC1 modulation (35), which could decrease signalling downstream of AKT. Taken together these results in GEMM of advanced localised PC demonstrate strong pre-clinical efficacy of the benefit of targeting signaling to the ribosome at multiple fronts.

Patient derived xenografts from multi-drug resistant CRPC metastasis are sensitive to dual inhibition of Pol I and PIM kinases

The current challenge in the treatment of advanced PC is the progression to late stage disease, CRPC and the development of resistance to novel AR targeting agents (36). Having demonstrated efficacy of our CX-5461/CX-6258 combination therapy in vitro and the Hi-MYC and PTEN-deficient *in vivo* models of PC, we tested the efficacy of this strategy using metastatic PC tissue obtained at autopsy. We used a patient derived xenograft (PDX) model in which thin slices of tissue are grafted under the renal capsule of immune deficient host mice. To take into account the heterogeneity of tissue during grafting, we devised a procedure (Figure 6A) whereby the tissue is sectioned and each contiguous slice is allocated to either a vehicle or drug treatment group. Considering, that this PDX approach requires that the whole experiment be done from the same starting graft due to tumor heterogeneity, it is not feasible to perform this experiment with more than two groups (e.g. vehicle vs. treatment). Using this approach we tested the combination of CX-5461 and CX-6258. Following engraftment, tumors were allowed to grow for 3 weeks followed by oral dosage over 9 days. Tumors were harvested and weighed (Figure 6B).

Comparison of graft weights from paired samples demonstrates a significant inhibition of tumor growth in the majority of drug treated samples. In 11 out of 16 pairs, the drug treated tumors had a lower weight than the corresponding vehicle treated tumor (Figure 6C) (P=0.04). Percentage of Ki-67 (Figure 6D) shows that these treated tumors have lower proliferation than vehicle treated pairs and increased cell death as marked by cleaved caspase-3 (Figure 6E). Considering that this tissue is derived from a metastasis isolated from a patient who failed to respond to conventional therapy and novel androgen targeted therapeutics, this significant result demonstrates the efficacy of this combination therapy in lethal PC.

Discussion

In this report, we describe the potential of RNA polymerase I transcription inhibition as a therapy for MYC-driven PC using a novel compound, CX-5461, in both human cells and GEMMs of PC that reflects the progression of human pathology. Pol I inhibition resulted in cell cycle arrest in human PC cell lines, even when p53 was mutated or lost, and this was associated with potent inhibition of colony formation in p53-null human lines and p53 wild type PC cells from the Hi-MYC mouse. These findings are consistent with our previous observation that the mutational status of p53 does not correlate with cell sensitivity to Pol I inhibition (26); however, it does significantly enhance inhibitor sensitivity (6). This is an important finding as loss-of-function p53 mutations are among the most common in PC, being present in roughly 50% of cases (37).

Clegg *et al.* (28) previously described the resistance of Hi-MYC mice to rapamycin. Additionally, Balakumaran *et al.* described that MYC-driven prostate cancer circumvents mTORC1 inhibition induced growth suppression because of incomplete or partial inhibition of mTORC1 (38), which most likely sustains or enhances 4EBP1 activity. Additionally, PIM-1 can mediate resistance by upregulating receptor tyrosine kinase activity in response to PI3K pathway

suppression (15). Although it remains unclear whether PIM kinases also mediate this resistance to therapy in Hi-MYC mice, PIM-1 was shown to be among the most significantly upregulated oncogenes in PC (17) and we show that significant phosphorylation of 4E-BP1 is observed in our Hi-MYC tumor cell line, HM-5, which could be relieved with CX-6258 administration. Interestingly, a recent study investigating MYC-driven colorectal tumorigenesis showed that targeting translation initiation bypasses this crosstalk signaling between MYC and mTOR resulting in reduced MYC levels in cancer (39).

Acute oral administration of CX-5461 and CX-6258 induced a 42% reduction in proliferative index in Hi-MYC adenocarcinoma and a remarkable decrease in the incidence of invasive tumor foci. It was recently described that PIM kinase inhibition had shown promising efficacy as a single agent in models of MYC-driven PC (30). In contrast, the results of our study do not show significant efficacy in a MYC-driven autochthonous PC model. However, the cooperation between CX-6258 and CX-5461 is consistent with the data of Kirschner *et al.*, showing that PIM kinase inhibition synergises well with agents that induce a p53 response in their mouse model of MYC-driven prostate cancer such as docetaxel and radiation therapy, standard therapies for recurrent PC (30). PTEN-deficiency is a feature of approximately 40% of PC (37), and here we show that this combination is also effective in a low MYC, PTEN deficiency-driven GEMM and PDX derived from human mCRPC. This is consistent with our hypothesis that this combination approach to targeting the ribosome will be efficacious in cancers featuring dysregulation of signalling via PI3K as well as MYC (40). To our knowledge, we are the first group to demonstrate that targeting ribosome biogenesis and ribosome function simultaneously can be exploited therapeutically in clinically relevant models of PC.

The data presented here strongly supports the idea that MYC confers tumor sensitivity to Pol I inhibition alone and treatment efficacy is remarkably enhanced when combined with PIM inhibition. These findings are significant as they demonstrate that MYC and PIM oncogenes are profoundly co-operative in PC and drive cell addiction to ribosome transcription and mRNA translation. This work supports the potential treatment of human prostate cancer with novel therapeutic agents, especially those resistant to conventional therapy and are characterised by MYC amplification. CX-5461 and pan-PIM inhibitors (41) are currently in phase 1 clinical trials for hematological malignancy.

Acknowledgments: We would like to thank Birunthi Niranjan for help with cell culture and Shelley Hedwards and Hong Wang for help with animal experiments.

References

1. Siegel RL, Miller KD, Jemal A. Cancer statistics, 2015. CA Cancer J Clin. 2015;65:5-29.
2. Karantanos T, Corn PG, Thompson TC. Prostate cancer progression after androgen deprivation therapy: mechanisms of castrate resistance and novel therapeutic approaches. Oncogene. 2013;32:5501-11.
3. Koh CM, Bieberich CJ, Dang CV, Nelson WG, Yegnasubramanian S, De Marzo AM. MYC and Prostate Cancer. Genes Cancer. 2010;1:617-28.
4. Gurel B, Iwata T, Koh CM, Jenkins RB, Lan F, Van Dang C, et al. Nuclear MYC protein overexpression is an early alteration in human prostate carcinogenesis. Mod Pathol. 2008;21:1156-67.
5. Hein N, Hannan KM, George AJ, Sanij E, Hannan RD. The nucleolus: an emerging target for cancer therapy. Trends Mol Med. 2013;19:643-54.
6. Poortinga G, Quinn LM, Hannan RD. Targeting RNA polymerase I to treat MYC-driven cancer. Oncogene. 2015;34:403-12.
7. Grandori C, Gomez-Roman N, Felton-Edkins ZA, Ngouenet C, Galloway DA, Eisenman RN, et al. c-Myc binds to human ribosomal DNA and stimulates transcription of rRNA genes by RNA polymerase I. Nat Cell Biol. 2005;7:311-8.
8. Uemura M, Zheng Q, Koh CM, Nelson WG, Yegnasubramanian S, De Marzo AM. Overexpression of ribosomal RNA in prostate cancer is common but not linked to rDNA promoter hypomethylation. Oncogene. 2012;31:1254-63.
9. Cibull TL, Jones TD, Li L, Eble JN, Ann Baldridge L, Malott SR, et al. Overexpression of Pim-1 during progression of prostatic adenocarcinoma. J Clin Pathol. 2006;59:285-8.
10. Zippo A, De Robertis A, Serafini R, Oliviero S. PIM1-dependent phosphorylation of histone H3 at serine 10 is required for MYC-dependent transcriptional activation and oncogenic transformation. Nat Cell Biol. 2007;9:932-44.
11. Zhang Y, Wang Z, Li X, Magnuson NS. Pim kinase-dependent inhibition of c-Myc degradation. Oncogene. 2008;27:4809-19.
12. Tamburini J, Green AS, Bardet V, Chapuis N, Park S, Willems L, et al. Protein synthesis is resistant to rapamycin and constitutes a promising therapeutic target in acute myeloid leukemia. Blood. 2009;114:1618-27.
13. Wang J, Kim J, Roh M, Franco OE, Hayward SW, Wills ML, et al. Pim1 kinase synergizes with c-MYC to induce advanced prostate carcinoma. Oncogene. 2010;29:2477-87.
14. Wang J, Anderson PD, Luo W, Gius D, Roh M, Abdulkadir SA. Pim1 kinase is required to maintain tumorigenicity in MYC-expressing prostate cancer cells. Oncogene. 2012;31:1794-803.
15. Cen B, Mahajan S, Wang W, Kraft AS. Elevation of receptor tyrosine kinases by small molecule AKT inhibitors in prostate cancer is mediated by Pim-1. Cancer research. 2013;73:3402-11.
16. Pourdehnad M, Truitt ML, Siddiqi IN, Ducker GS, Shokat KM, Ruggero D. Myc and mTOR converge on a common node in protein synthesis control that confers synthetic lethality in Myc-driven cancers. Proc Natl Acad Sci U S A. 2013;110:11988-93.
17. Ellwood-Yen K, Graeber TG, Wongvipat J, Iruela-Arispe ML, Zhang J, Matusik R, et al. Myc-driven murine prostate cancer shares molecular features with human prostate tumors. Cancer cell. 2003;4:223-38.

18. Takizawa I, Lawrence MG, Balanathan P, Rebello R, Pearson HB, Garg E, et al. Estrogen receptor alpha drives proliferation in PTEN-deficient prostate carcinoma by stimulating survival signaling, MYC expression and altering glucose sensitivity. Oncotarget. 2015;6:604-16.
19. Furic L, Rong L, Larsson O, Koumakpayi IH, Yoshida K, Brueschke A, et al. eIF4E phosphorylation promotes tumorigenesis and is associated with prostate cancer progression. Proceedings of the National Academy of Sciences of the United States of America. 2010;107:14134-9.
20. Jin C, McKeehan K, Wang F. Transgenic mouse with high Cre recombinase activity in all prostate lobes, seminal vesicle, and ductus deferens. The Prostate. 2003;57:160-4.
21. Lesche R, Groszer M, Gao J, Wang Y, Messing A, Sun H, et al. Cre/loxP-mediated inactivation of the murine Pten tumor suppressor gene. Genesis. 2002;32:148-9.
22. Bywater MJ, Poortinga G, Sanij E, Hein N, Peck A, Cullinane C, et al. Inhibition of RNA polymerase I as a therapeutic strategy to promote cancer-specific activation of p53. Cancer cell. 2012;22:51-65.
23. Poortinga G, Wall M, Sanij E, Siwicki K, Ellul J, Brown D, et al. c-MYC coordinately regulates ribosomal gene chromatin remodeling and Pol I availability during granulocyte differentiation. Nucleic Acids Res. 2011;39:3267-81.
24. Lawrence MG, Taylor RA, Toivanen R, Pedersen J, Norden S, Pook DW, et al. A preclinical xenograft model of prostate cancer using human tumors. Nat Protoc. 2013;8:836-48.
25. Liu C, Zhu Y, Lou W, Nadiminty N, Chen X, Zhou Q, et al. Functional p53 determines docetaxel sensitivity in prostate cancer cells. The Prostate. 2013;73:418-27.
26. Drygin D, Lin A, Bliesath J, Ho CB, O'Brien SE, Proffitt C, et al. Targeting RNA polymerase I with an oral small molecule CX-5461 inhibits ribosomal RNA synthesis and solid tumor growth. Cancer research. 2011;71:1418-30.
27. Wong YC, Tam NN. Dedifferentiation of stromal smooth muscle as a factor in prostate carcinogenesis. Differentiation. 2002;70:633-45.
28. Clegg NJ, Couto SS, Wongvipat J, Hieronymus H, Carver BS, Taylor BS, et al. MYC cooperates with AKT in prostate tumorigenesis and alters sensitivity to mTOR inhibitors. PloS one. 2011;6:e17449.
29. Chen WW, Chan DC, Donald C, Lilly MB, Kraft AS. Pim family kinases enhance tumor growth of prostate cancer cells. Mol Cancer Res. 2005;3:443-51.
30. Kirschner AN, Wang J, van der Meer R, Anderson PD, Franco-Coronel OE, Kushner MH, et al. PIM kinase inhibitor AZD1208 for treatment of MYC-driven prostate cancer. Journal of the National Cancer Institute. 2015;107.
31. Haddach M, Michaux J, Schwaebe MK, Pierre F, O'Brien SE, Borsan C, et al. Discovery of CX-6258. A Potent, Selective, and Orally Efficacious pan-Pim Kinases Inhibitor. ACS Med Chem Lett. 2012;3:135-9.
32. Shapiro GI, Harper JW. Anticancer drug targets: cell cycle and checkpoint control. J Clin Invest. 1999;104:1645-53.
33. Trotman LC, Niki M, Dotan ZA, Koutcher JA, Di Cristofano A, Xiao A, et al. Pten dose dictates cancer progression in the prostate. PLoS Biol. 2003;1:E59.
34. Wang S, Gao J, Lei Q, Rozengurt N, Pritchard C, Jiao J, et al. Prostate-specific deletion of the murine Pten tumor suppressor gene leads to metastatic prostate cancer. Cancer cell. 2003;4:209-21.

35. Lu J, Zavorotinskaya T, Dai Y, Niu XH, Castillo J, Sim J, et al. Pim2 is required for maintaining multiple myeloma cell growth through modulating TSC2 phosphorylation. Blood. 2013;122:1610-20.
36. Mukherji D, Omlin A, Pezaro C, Shamseddine A, de Bono J. Metastatic castration-resistant prostate cancer (CRPC): preclinical and clinical evidence for the sequential use of novel therapeutics. Cancer metastasis reviews. 2014;33:555-66.
37. Robinson D, Van Allen EM, Wu YM, Schultz N, Lonigro RJ, Mosquera JM, et al. Integrative clinical genomics of advanced prostate cancer. Cell. 2015;161:1215-28.
38. Balakumaran BS, Porrello A, Hsu DS, Glover W, Foye A, Leung JY, et al. MYC activity mitigates response to rapamycin in prostate cancer through eukaryotic initiation factor 4E-binding protein 1-mediated inhibition of autophagy. Cancer research. 2009;69:7803-10.
39. Wiegering A, Uthe FW, Jamieson T, Ruoss Y, Huttenrauch M, Kuspert M, et al. Targeting translation initiation bypasses signaling crosstalk mechanisms that maintain high MYC levels in colorectal cancer. Cancer Discov. 2015.
40. Devlin JR, Hannan KM, Hein N, Cullinane C, Kusnadi E, Ng PY, et al. Combination Therapy Targeting Ribosome Biogenesis and mRNA Translation Synergistically Extends Survival in MYC-Driven Lymphoma. Cancer discovery. 2016;6:59-70.
41. Keeton EK, McEachern K, Dillman KS, Palakurthi S, Cao Y, Grondine MR, et al. AZD1208, a potent and selective pan-Pim kinase inhibitor, demonstrates efficacy in preclinical models of acute myeloid leukemia. Blood. 2014;123:905-13.

Figure legends

Fig. 1. CX-5461 inhibits the anchorage-independent growth of PC cells and induces cell cycle arrest independent of p53 status. (A) Western blotting analysis of protein extracts from human (HPE-1, HPE-2, PC3, DU145, LNCaP) and mouse (BM67, HM-5) prostate cancer cell lines showing MYC expression with β-actin as a loading control. **(B)** The relative number of colonies suspended in low melt agarose of PC-3 and **(C)** DU145 cells after 3 weeks incubation with CX-5461 (red & blue) or vehicle only (black) (mean ± SD, **P*<0.0001). **(D)** The percentage of PC-3 and **(E)** DU145 cells in each cell cycle phase after 24hrs incubation with increasing concentrations of CX-5461 (red & blue) or vehicle only (black) (n=3, mean ± SD). **(F)** The percentage of LNCaP cells in each cell cycle phase after 48 hrs incubation with increasing concentrations of CX-5461 (green) or vehicle only (black). **(G)** Western blotting analysis of protein extracts from LNCaP cells showing expression of p53 and p21 after 30 min, 2, 4, 8 and 24 hours after administration of CX-5461.

Fig. 2. CX-5461 inhibits ribosomal DNA transcription and MYC-driven cell proliferation *in vivo*, in Hi-MYC prostate adenocarcinoma. (A) Representative images of wild type (WT) or Hi-MYC lateral prostate from 2, 5 and 8 month old mice, immunohistochemically stained for α-smooth muscle actin (α-SMA) (Arrows mark fragmented smooth muscle, scale bars = 100 μm) **(B)** The percentage of MYC (upper) and Ki-67 (lower) positive cells analysed by IHC at each age described (n=3 per group, mean ± SD, **P* <0.05). **(C)** The relative expression of 45S precursor rRNA from 5 month old Hi-MYC lateral prostate (Hi-MYC LP) isolated from mice 0, 8 and 24 hrs after an oral dose of 50 mg/kg CX-5461 (n=3 per group, mean ± SD, paired t-test **P*=0.05). **(D)** The expression of p53 protein in Hi-MYC LP isolated from mice 2, 4, 8, 12 and 24 hrs after an oral dose of 50mg/kg CX-5461. **(E, F)** Representative images and **(G, H)**

quantitation of 5 month old Hi-MYC LP showing IHC for MYC and Ki-67 respectively after isolation from mice given longer term therapy with CX-5461 (50 mg/kg, bi-weekly, 9 doses, Scale bars = 100 μm) (n=3, mean ± SD, t-test *P=0.02).

Fig. 3. CX-5461 co-operates with pan-PIM kinases inhibitor, CX-6258, in PC cell lines.

(A) The relative number of colonies suspended in low melt agarose of PC3 and **(B)** DU145 cells after 3 weeks incubation with CX-6258 (red & blue) or vehicle only (black) (mean ± SD, *P<0.01, ** P<0.001, *** P<0.0001). **(C)** The percentage of LNCaP cells in each phase of the cell cycle after 48 hrs incubation in the presence of CX-6258 (mean ± SD, **P<0.01, ****P<0.0001). **(D)** Western blotting analysis of PC3 and DU145 cell extracts after 2 hours incubation with either 0, 5 or 10 μM CX-6258 or 10 μM CX-5461. These blots were probed for the expression of MYC, phosphorylated 4E-BP1 (s65), total 4E-BP1 and β-actin (loading control). **(E)** The relative number of colonies suspended in low melt agarose of PC3 and **(F)** DU145 cells after 3 weeks incubation with a single agent or in combination or vehicle only (mean ± SEM, *p<0.01, **p<0.001, ***p<0.0001). The percentage of **(G)** LNCaP and **(H)** DU145 cells in each phase of the cell cycle after 24 hrs incubation with either single agent alone or in combination (*P≤0.05, **P<0.01, ***P<0.001, ****P<0.0001).

Fig. 4. Combined inhibition induces p53 mediated cell cycle arrest and death in a Hi-MYC tumor cell line. (A) The relative abundance of 45S pre-rRNA as marked by 5' Internal transcribed spacer 1 (ITS1) after 1 hr incubation with CX-5461 in a 5 month old Hi-MYC tumor cell line (HM-5) (mean ± SD, ANOVA **P<0.01, ****P<0.0001). **(B)** Western blotting analysis showing the expression of p53 after 1hr incubation with increasing doses of CX-5461 in HM-5 cells. **(C)** The relative abundance of p21 mRNA after 1 hr incubation with increasing doses of CX-5461 (mean ± SD, ANOVA *P<0.05 **P<0.01 ***P<0.001). **(D)** The number of cells in

each phase of the cell cycle after incubation with either CX-5461, CX-6258 or in combination for 24 hrs (mean ± SD, ANOVA *$P \leq 0.05$). **(E)** Western blotting analysis of the change in MYC, PIM-1, phosphorylated 4E-BP1 (s65), total 4E-BP1 and β-actin (loading control) expression after 2 hrs incubation with increasing doses of CX-6258. **(F)** The relative number of cells after incubation with 10 nM CX-5461, 200 nM CX-6258 or a combination of inhibitors for 72 hrs (mean ± SD, ANOVA *p<0.05 **p<0.01). **(G)** The relative number of colonies suspended in 2% matrigel after incubation with CX-5461, CX-6258 or a combination of inhibitors (mean ± SD, ANOVA *p<0.05). **(H)** The percentage of dead cells after 72hrs incubation with a single dose of CX-5461, CX-6258 or in combination (mean ± SD, ANOVA *p<0.05 **p<0.01).

Fig. 5 CX-5461 co-operates with pan-PIM kinases inhibitor CX-6258, *in vivo*, to inhibit proliferation and incidence of invasive carcinoma. (A) Representative images at low (4X) and high (10X) magnification of α-smooth muscle actin (α-SMA) IHC of 5 month old Hi-MYC mice orally dosed with either Vehicle (n=11), CX-5461 (n=8), CX-6258 (n=8) single agents alone or in combination (n=11) (bi-weekly, 9 doses). Arrows mark fragmented smooth muscle actin. Scale bars = 100 μm **(B)** The percentage of invasive lesions in Hi-MYC LP as a proportion of total lesions (invasive & non-invasive) marked by the loss of α-SMA. Each point represents an individual mouse, blindly quantified for lesions. **(C)** The percentage of cells positive Ki-67 in representative Hi-MYC lateral prostate sections (mean difference analysed by ANOVA, Dunnett's post hoc, *P<0.05). **(D)** Representative images of low (2X) and high (20X) magnification of 5 month old anterior prostate from PTEN deficient (PBiCre+;PtenFl/Fl) mice dosed with either Vehicle (n=4), CX-5461 (n=4), CX-6258 (n=4) or in combination (n=4) (bi-weekly, 9 doses). **(E)** The percentage of *in situ* carcinoma in these mice 24 hours after final dosage. Each point represents an individual mouse.

Fig. 6 Combination therapy inhibits tumor growth in high-MYC mCRPC patient-derived xenografts. (A) The PDX technique involves cutting the tissue into thin slices (0.3 mm) using an automated live tissue microtome and regrafting slices across all recipient mice, noting the numerical order of each slice and the position of the graft on each kidney. For each drug treatment, a minimum of 8 mice is required (4 vehicle and 4 controls). Tumors were allowed to grow on the kidney of NSG recipient mice for 3 weeks before drug treatment via gavage for 2 weeks. At time of collection, the volume of each harvested graft is measured with a calliper and also weighed. **(B)** Graphical analysis is plotted as contiguous tumors generated from the original graft. Impact of tumor growth is analysed by comparing the weight of each drug combination treated graft to the previous vehicle-only treated graft in sequential order of sectioned slices. This approach allows us to control for heterogeneity or polyclonality in the precursor tumor. **(C)** Differences in weight obtained from graft pairs (drug treated vs. vehicle) from contiguous slices. (**P*=0.04). **(D)** Differences in Ki-67 ($p<0.001$) and **(E)** cleaved caspase-3 ($p=0.02$) percentage between graft pairs (drug treated vs. vehicle) from contiguous slices. Statistical analysis is performed using the Wilcoxon signed-rank test for paired observations (contiguous tissue slices).

Figure 1

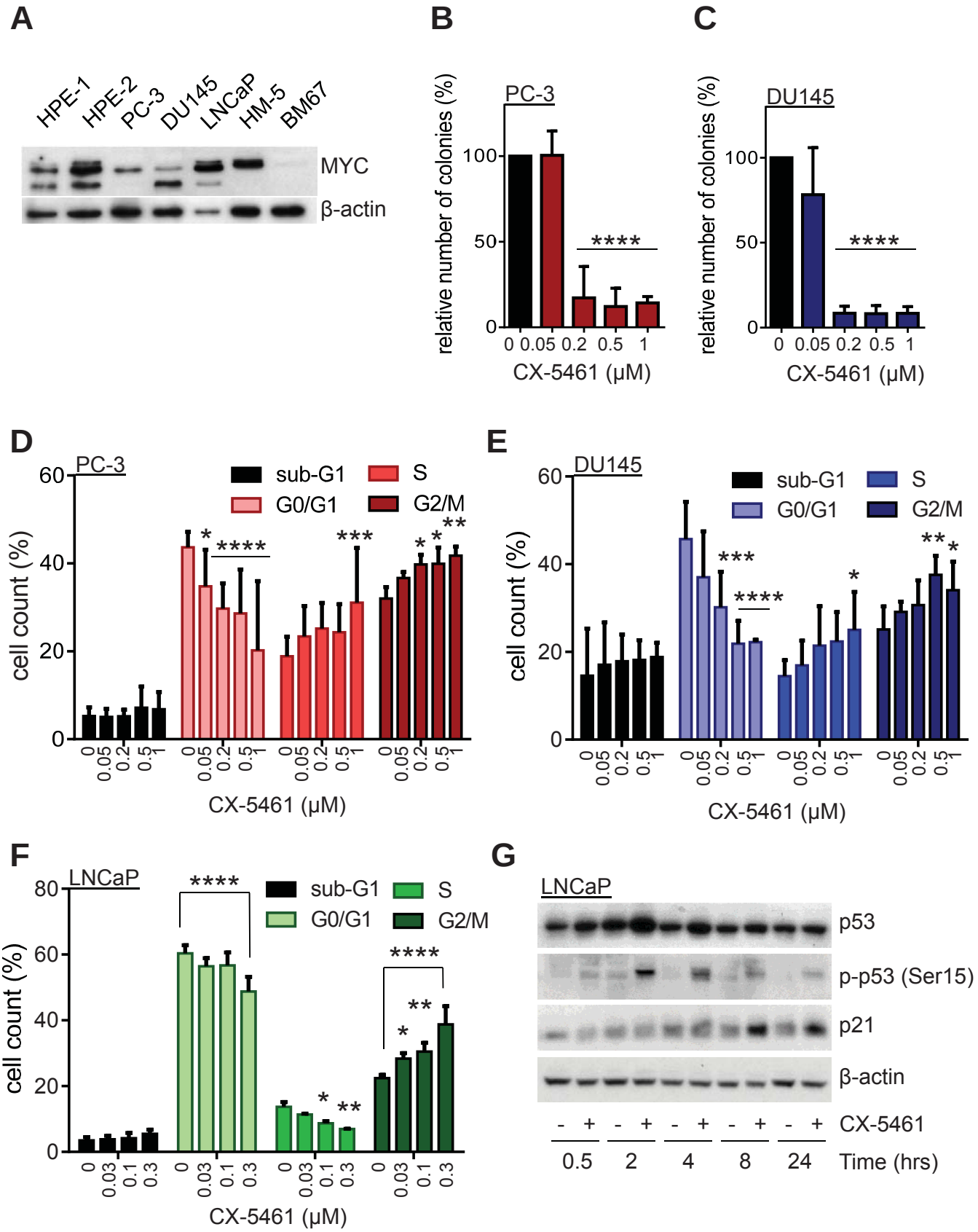
A
HPE-1
HPE-2
PC-3
DU145
LNCaP
HM-5
BM67
MYC
β-actin
B
PC-3
relative number of colonies (%)
100
50
0
****
0 0.05 0.2 0.5 1
CX-5461 (μM)
C
DU145
relative number of colonies (%)
100
50
0
****
0 0.05 0.2 0.5 1
CX-5461 (μM)
D
PC-3
sub-G1
S
G0/G1
G2/M
cell count (%)
60
40
20
0
CX-5461 (μM)
E
DU145
sub-G1
S
G0/G1
G2/M
cell count (%)
60
40
20
0
CX-5461 (μM)
F
LNCaP
sub-G1
S
G0/G1
G2/M
cell count (%)
80
60
40
20
0
****
CX-5461 (μM)
G
LNCaP
p53
p-p53 (Ser15)
p21
β-actin
- + - + - + - + - + CX-5461
0.5 2 4 8 24 Time (hrs)

Figure 2

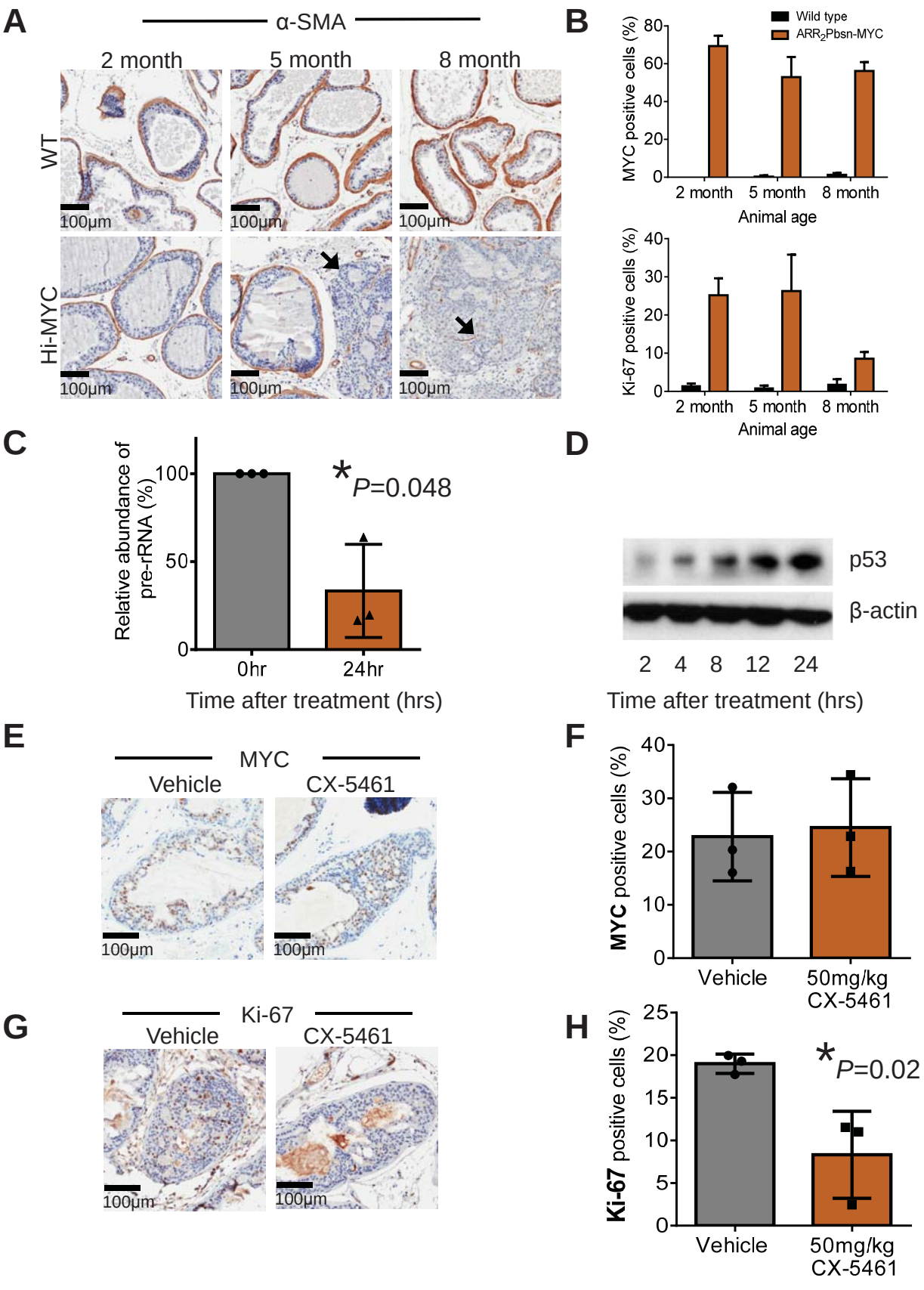
A
α-SMA
2 month
5 month
8 month
WT
Hi-MYC
100μm
B
Wild type
ARR2Pbsn-MYC
MYC positive cells (%)
Ki-67 positive cells (%)
2 month
5 month
8 month
Animal age
C
Relative abundance of pre-rRNA (%)
*P=0.048
0hr
24hr
Time after treatment (hrs)
D
p53
β-actin
2 4 8 12 24
Time after treatment (hrs)
E
MYC
Vehicle
CX-5461
F
MYC positive cells (%)
Vehicle
50mg/kg CX-5461
G
Ki-67
Vehicle
CX-5461
H
Ki-67 positive cells (%)
*P=0.02
Vehicle
50mg/kg CX-5461

Figure 3

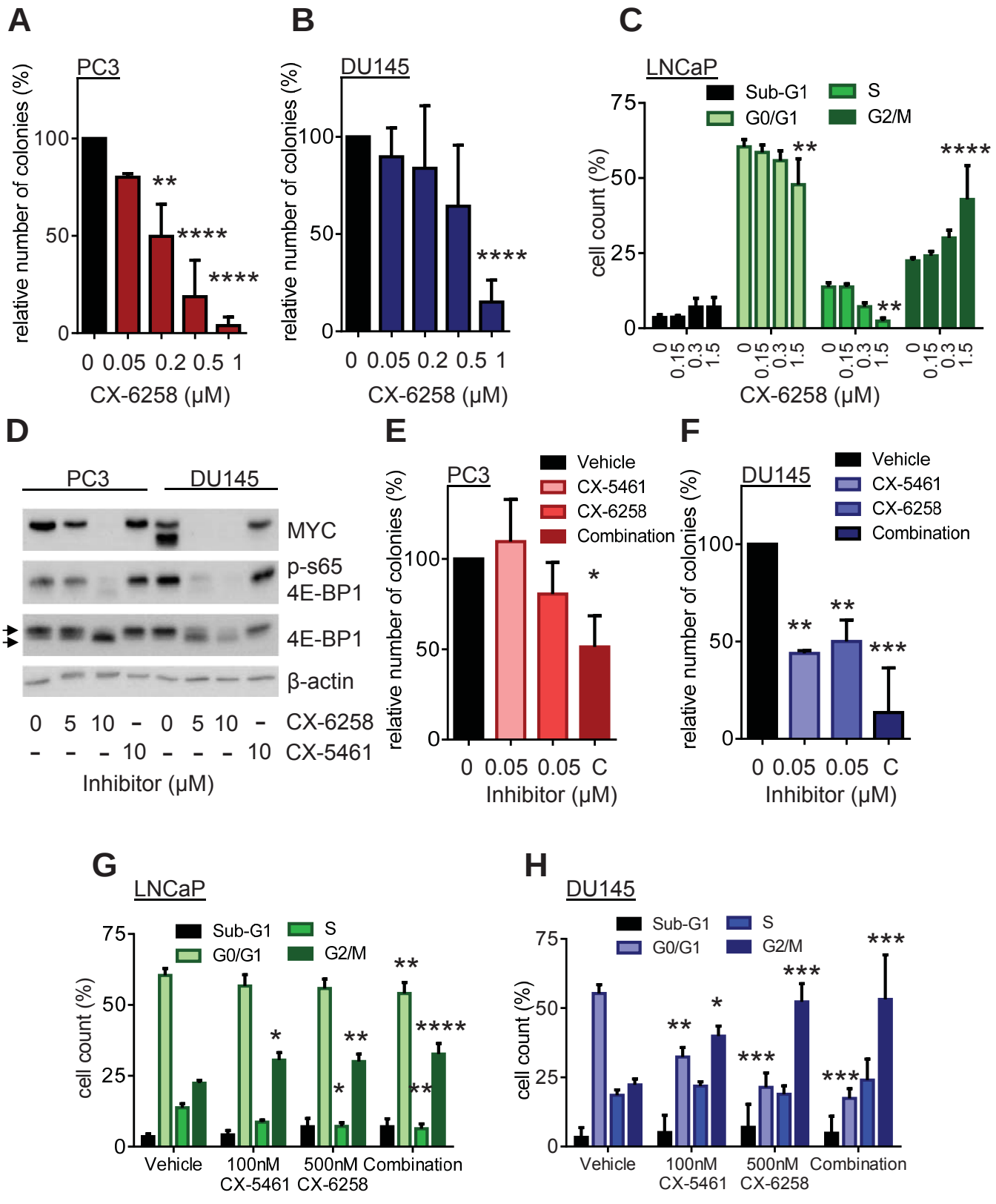
A
PC3
relative number of colonies (%)
100
50
0
**
****
****
0 0.05 0.2 0.5 1
CX-6258 (μM)
B
DU145
relative number of colonies (%)
100
50
0
****
0 0.05 0.2 0.5 1
CX-6258 (μM)
C
LNCaP
Sub-G1
G0/G1
S
G2/M
cell count (%)
75
50
25
0
**
**
****
0 0.15 0.3 1.5
CX-6258 (μM)
D
PC3
DU145
MYC
p-s65 4E-BP1
4E-BP1
β-actin
0 5 10 – 0 5 10 – CX-6258
– – – 10 – – – 10 CX-5461
Inhibitor (μM)
E
PC3
Vehicle
CX-5461
CX-6258
Combination
relative number of colonies (%)
100
50
0
*
0 0.05 0.05 C
Inhibitor (μM)
F
DU145
Vehicle
CX-5461
CX-6258
Combination
relative number of colonies (%)
100
50
0
**
**
***
0 0.05 0.05 C
Inhibitor (μM)
G
LNCaP
Sub-G1
G0/G1
S
G2/M
cell count (%)
75
50
25
0
*
**
*
**
**
****
Vehicle
100nM CX-5461
500nM CX-6258
Combination
H
DU145
Sub-G1
G0/G1
S
G2/M
cell count (%)
75
50
25
0
**
*
***
***
***
***
Vehicle
100nM CX-5461
500nM CX-6258
Combination

Figure 4

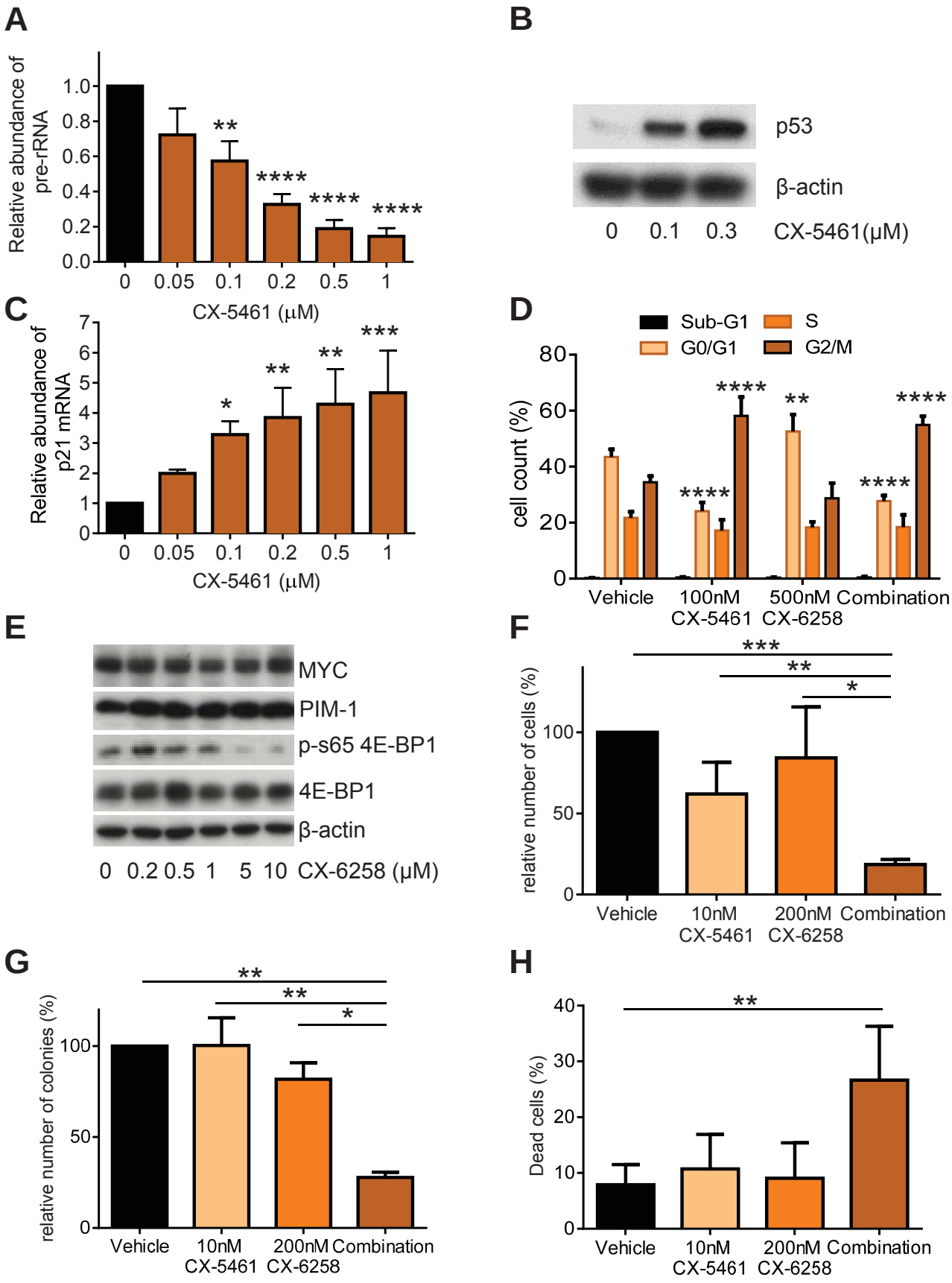
A
Relative abundance of pre-rRNA
1.0
0.8
0.6
0.4
0.2
0.0
**
****
****
****
0
0.05
0.1
0.2
0.5
1
CX-5461 (μM)
B
p53
β-actin
0
0.1
0.3
CX-5461(μM)
C
Relative abundance of p21 mRNA
7
6
5
4
3
2
1
0
*
**
**
***
0
0.05
0.1
0.2
0.5
1
CX-5461 (μM)
D
Sub-G1
S
G0/G1
G2/M
cell count (%)
80
60
40
20
0
****
****
**
****
Vehicle
100nM CX-5461
500nM CX-6258
Combination
E
MYC
PIM-1
p-s65 4E-BP1
4E-BP1
β-actin
0
0.2
0.5
1
5
10
CX-6258 (μM)
F
relative number of cells (%)
100
50
0
***
**
*
Vehicle
10nM CX-5461
200nM CX-6258
Combination
G
relative number of colonies (%)
100
50
0
**
**
*
Vehicle
10nM CX-5461
200nM CX-6258
Combination
H
Dead cells (%)
40
30
20
10
0
**
Vehicle
10nM CX-5461
200nM CX-6258
Combination

Figure 5

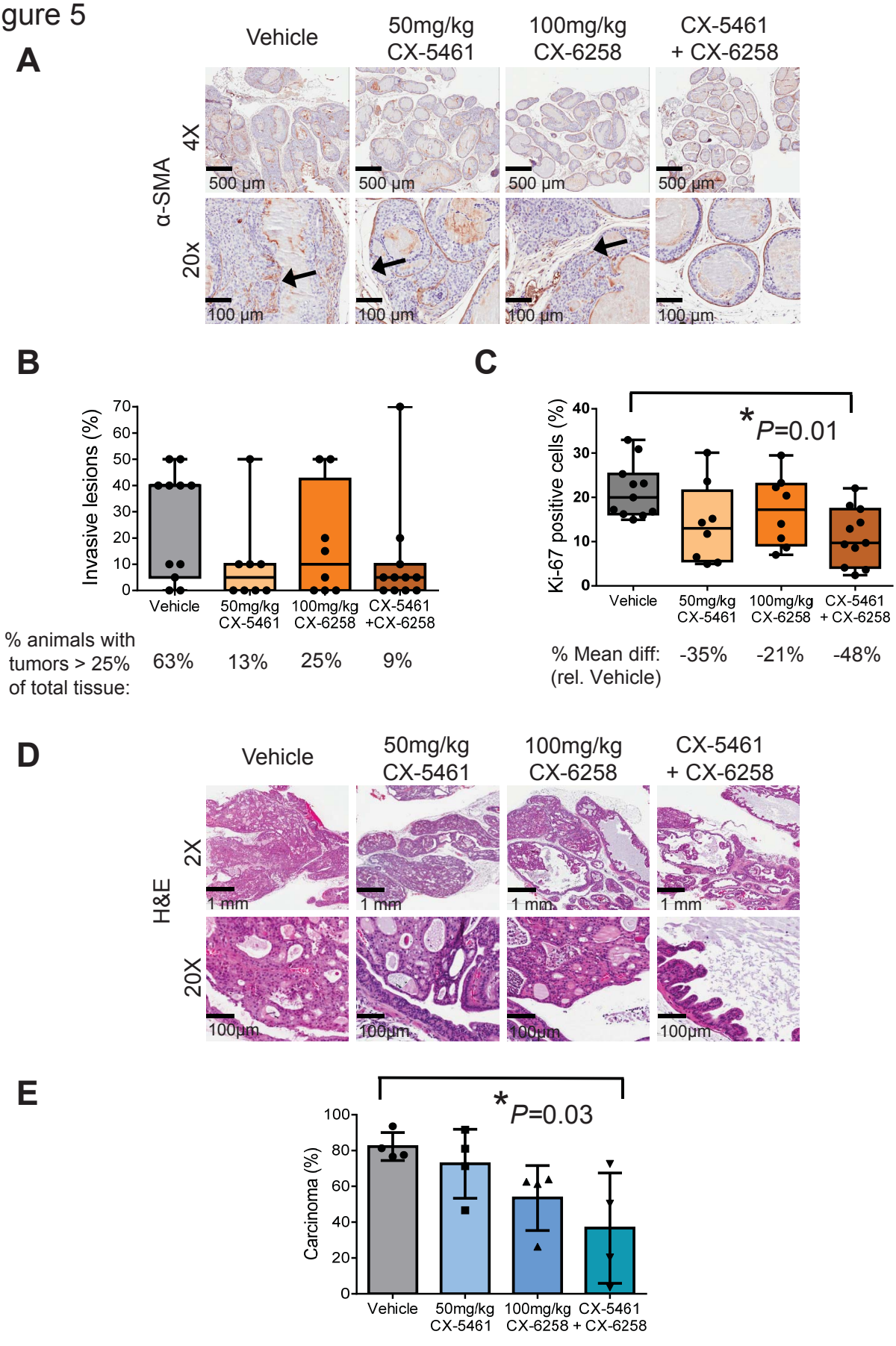
A
Vehicle
50mg/kg CX-5461
100mg/kg CX-6258
CX-5461 + CX-6258
α-SMA
4X
20x
500 µm
100 µm
B
Invasive lesions (%)
Vehicle
50mg/kg CX-5461
100mg/kg CX-6258
CX-5461 +CX-6258
% animals with tumors > 25% of total tissue:
63%
13%
25%
9%
C
Ki-67 positive cells (%)
*P=0.01
Vehicle
50mg/kg CX-5461
100mg/kg CX-6258
CX-5461 + CX-6258
% Mean diff: (rel. Vehicle)
-35%
-21%
-48%
D
Vehicle
50mg/kg CX-5461
100mg/kg CX-6258
CX-5461 + CX-6258
H&E
2X
20X
1 mm
100µm
E
Carcinoma (%)
*P=0.03
Vehicle
50mg/kg CX-5461
100mg/kg CX-6258 + CX-6258

Figure 6

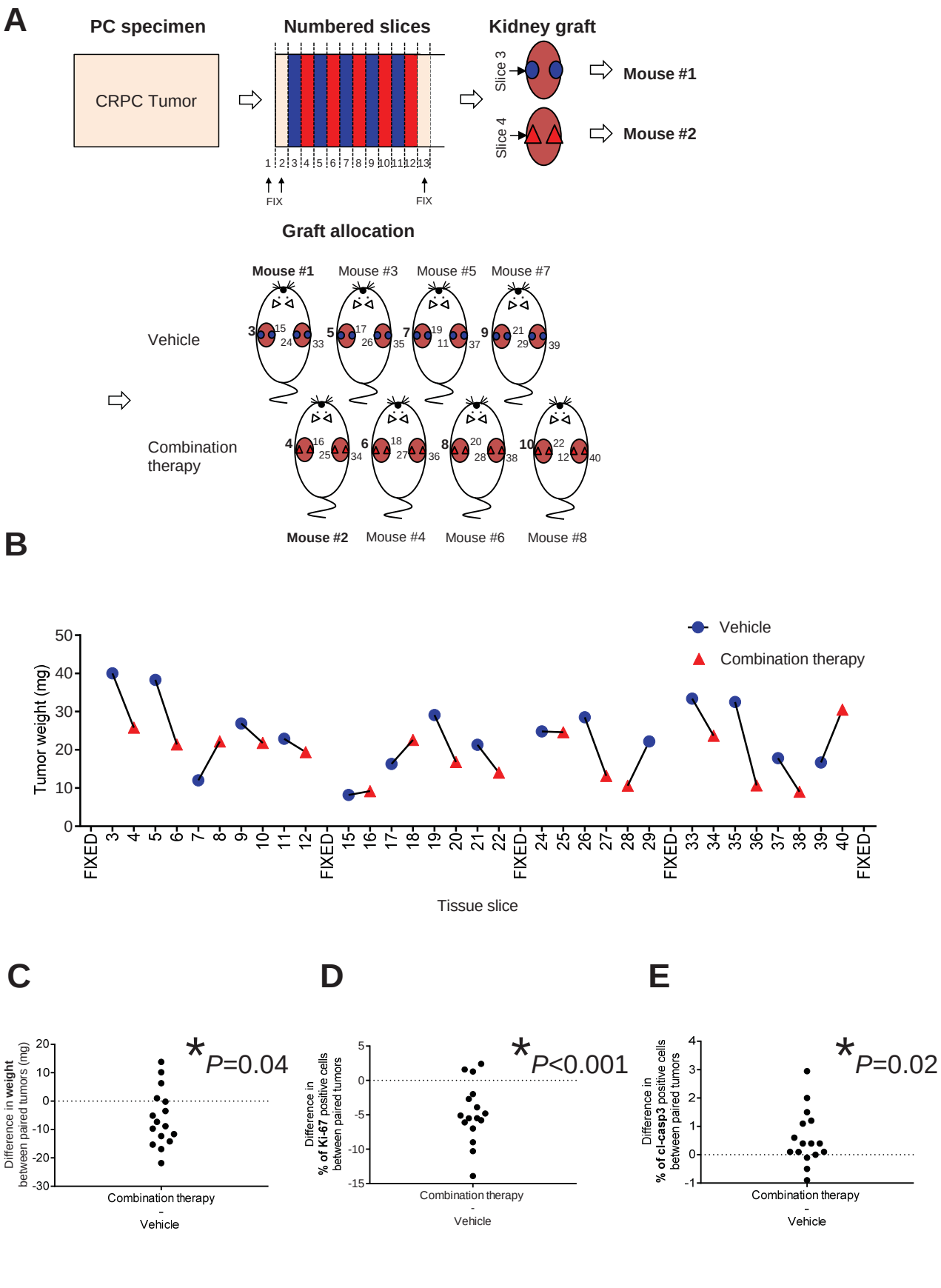
A
PC specimen
CRPC Tumor
Numbered slices
1 2 3 4 5 6 7 8 9 10 11 12 13
FIX
FIX
Kidney graft
Slice 3
Slice 4
Mouse #1
Mouse #2
Graft allocation
Mouse #1
Mouse #3
Mouse #5
Mouse #7
Vehicle
3 15 24 33
5 17 26 35
7 19 11 37
9 21 29 39
Combination therapy
4 16 25 34
6 18 27 36
8 20 28 38
10 22 12 40
Mouse #2
Mouse #4
Mouse #6
Mouse #8
B
Vehicle
Combination therapy
Tumor weight (mg)
0
10
20
30
40
50
FIXED 3 4 5 6 7 8 9 10 11 12 FIXED 15 16 17 18 19 20 21 22 FIXED 24 25 26 27 28 29 FIXED 33 34 35 36 37 38 39 40 FIXED
Tissue slice
C
Difference in weight between paired tumors (mg)
20
10
0
-10
-20
-30
*P=0.04
Combination therapy
-
Vehicle
D
Difference in % of Ki-67 positive cells between paired tumors
5
0
-5
-10
-15
*P<0.001
Combination therapy
-
Vehicle
E
Difference in % of cl-casp3 positive cells between paired tumors
4
3
2
1
0
-1
*P=0.02
Combination therapy
-
Vehicle